

Science

 AAAS

Gate-Variable Optical Transitions in Graphene

Feng Wang, *et al.*

Science **320**, 206 (2008);

DOI: 10.1126/science.1152793

The following resources related to this article are available online at www.sciencemag.org (this information is current as of January 12, 2009):

Updated information and services, including high-resolution figures, can be found in the online version of this article at:

<http://www.sciencemag.org/cgi/content/full/320/5873/206>

Supporting Online Material can be found at:

<http://www.sciencemag.org/cgi/content/full/1152793/DC1>

This article **cites 19 articles**, 6 of which can be accessed for free:

<http://www.sciencemag.org/cgi/content/full/320/5873/206#otherarticles>

This article appears in the following **subject collections**:

Physics, Applied

http://www.sciencemag.org/cgi/collection/app_physics

Information about obtaining **reprints** of this article or about obtaining **permission to reproduce this article** in whole or in part can be found at:

<http://www.sciencemag.org/about/permissions.dtl>

Gate-Variable Optical Transitions in Graphene

Feng Wang,^{1*} Yuanbo Zhang,¹ Chuanshan Tian,¹ Caglar Girit,^{1,2} Alex Zettl,^{1,2} Michael Crommie,^{1,2} Y. Ron Shen^{1,2}

Two-dimensional graphene monolayers and bilayers exhibit fascinating electrical transport behaviors. Using infrared spectroscopy, we find that they also have strong interband transitions and that their optical transitions can be substantially modified through electrical gating, much like electrical transport in field-effect transistors. This gate dependence of interband transitions adds a valuable dimension for optically probing graphene band structure. For a graphene monolayer, it yields directly the linear band dispersion of Dirac fermions, whereas in a bilayer, it reveals a dominating van Hove singularity arising from interlayer coupling. The strong and layer-dependent optical transitions of graphene and the tunability by simple electrical gating hold promise for new applications in infrared optics and optoelectronics.

Graphene, a single layer of honeycomb carbon lattice, exhibits many exotic behaviors, ranging from the anomalous quantum Hall effect (1–3) and Klein paradox (4) to coherent transport (5). In contrast to the extensive effort on electrical transport, optical study of graphene has been limited (6–9). Such optical investigation is important for understanding the electronic structures and excited-state properties of low-dimensional materials, as recently demonstrated in the case of carbon nanotubes, for example (10, 11).

We have used infrared (IR) spectroscopy to probe interband optical transitions in monolayers and bilayers of graphene, which show distinctly different optical response. Unlike conventional materials, the optical transitions in graphene can be dramatically modified through electrical gating: The normalized gate-induced changes in transition strengths approach the order of unity. Although field-effect-modulated electrical conductivity has long been the basis of modern electronics, such large modification of optical transitions by electrical gating is unusual. (For comparison, relative refractive index change in typical electro-optical materials rarely reaches 10^{-3} .) The special behavior of graphene is due both to its two-dimensional (2D) structure that confines electrons in one atomic layer and to its low density of states (DOS) near the Dirac point, which causes the Fermi energy (E_F) to shift significantly with variation of carrier density.

The strong gate dependence of optical transitions allows detailed examination of graphene band structure. We observed the linear Dirac band in graphene monolayer and were able to determine through direct optical means the band dispersion. For a graphene bilayer, we observed a dominating van Hove singularity that results from interlayer band hybridization, and our results in-

dicating that many-body effects may play a role in the excited-state properties of graphene. Aside from such fundamental interests, the very unusual optical properties of graphene make it a promising material for IR optoelectronics. This is particularly attractive considering that graphene possesses superior carrier mobility, current carrying capability, and thermal conductivity, and can readily incorporate electrical coupling as in field-effect devices (12) and pn junctions (13, 14).

We prepared mechanically exfoliated graphene monolayer and bilayer samples on heavily doped Si/SiO₂ substrates by following the peeling procedure described in (12). Monolayers and bilayers of graphene were identified with an optical microscope and subsequently confirmed by Raman spectroscopy (6). On some of the samples, we attached a gold electrode (thickness ~30 nm) by deposition in a vacuum through a mask. The heavily doped Si underneath the 290-nm-thick SiO₂ served as a back gate, which allowed us to tune the charge carrier density in the graphene samples.

We investigated the graphene interband transitions using IR reflection spectroscopy in a mi-

croscopic setup at room temperature (15). Two types of measurements were performed. To probe optical transitions of graphene monolayers and bilayers, we measured the normalized change of IR reflectivity $\delta R/R$ from the sample with reference to the bare substrate, achieved by modulating the sample position such that the graphene film on the substrate was shifted in and out of the beam spot. To examine the gate dependence of the optical transitions, we fixed the sample position and applied a dc gate on the graphene sample. A small ac modulation was added to the dc gate voltage, and the modulated reflectivity change at the ac modulation frequency was detected by a lockin amplifier. The result yielded $\frac{\partial(\delta R/R)}{\partial V}$, the derivative of $\delta R/R$ with respect to the gate voltage V .

We plot in Fig. 1A the measured $-\delta R/R$ versus photon energy for a representative graphene monolayer (blue circle) and graphene bilayer (red square), whose optical microscopy images are displayed in Fig. 1, B and C, respectively. Note that $\delta R/R$ is related to the complex optical conductivity $\sigma(\omega)$ of graphene through the relation:

$$-\frac{\delta R}{R} = \frac{1}{c} \text{Re}[\eta \cdot \sigma] \quad (1)$$

where η is a dimensionless complex factor that includes an interfering contribution from substrate reflection and can be calculated exactly (16). The observed spectra of graphene monolayers and bilayers differ dramatically. The difference can be qualitatively understood from their different electronic band structures.

The graphene monolayer spectrum is basically featureless, which is consistent with the linear electronic bands (Fig. 1D). In fact, the absorption coefficient of an undoped graphene layer in the IR region is expected to be strictly a constant (17, 18). The observed $-\delta R/R$, related but not proportional to graphene absorption, ac-

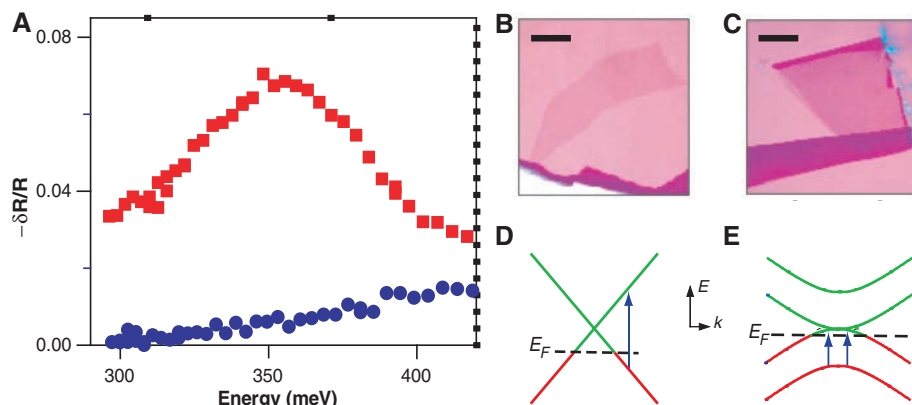


Fig. 1. (A) Normalized change of IR reflectivity $-\delta R/R$ referenced to the bare substrate for a graphene monolayer (blue circles) and bilayer (red squares). (B and C) Optical microscopy image of a graphene monolayer and bilayer, respectively, on a SiO₂/Si substrate. The scale bars are 20 μm . (D and E) Band structures of monolayer and AB stacking bilayer of graphene, respectively. The graphene samples are hole-doped. The linear bands of graphene monolayer produce a relatively flat $-\delta R/R$ spectrum, and the parallel bands of graphene bilayer lead to a peak in the $-\delta R/R$ spectrum.

¹Department of Physics, University of California at Berkeley, Berkeley, CA 94720, USA. ²Materials Science Division, Lawrence Berkeley National Laboratory, Berkeley, CA 94720, USA.

*To whom correspondence should be addressed. E-mail: fengwang76@berkeley.edu

quires slow wavelength dependence in the region we investigated, partly from dispersion in η of Eq. 1 and partly from free carrier response due to p-doping of the as-prepared exfoliated graphenes.

The bilayer electronic structure is affected by orbital hybridization between the adjacent layers. For a bilayer with AB stacking, tight-binding calculations predict two parallel conduction bands and two parallel valence bands. The band gap is zero, and the parallel band separation corresponds to the interlayer nearest-neighbor hopping rate γ_1 (Fig. 1E) (19–22). Both features are unique characteristics of the bilayer. The optical transitions between the parallel valence bands (indicated by the arrowed

lines in Fig. 1E) lead to a strong van Hove singularity. They are allowed in bilayers that are p-doped. Indeed, our $-\delta R/R$ spectrum for the bilayer exhibits a clear peak around 350 meV, near the parallel band separation of 400 meV determined by photoemission (21, 23).

The gate dependence of these optical transitions provides an extra dimension of information. A 2D plot (Fig. 2A) of the experimentally measured $\partial(\delta R/R)/\partial V$ as a function of probing photon energy and dc gate voltage for a graphene monolayer shows two main features. First, for a given photon energy, the absolute value of $\partial(\delta R/R)/\partial V$ has a maximum at a certain gate voltage, as can be seen from a vertical cut of the 2D plot (symbols in Fig. 2C). Second, the gate

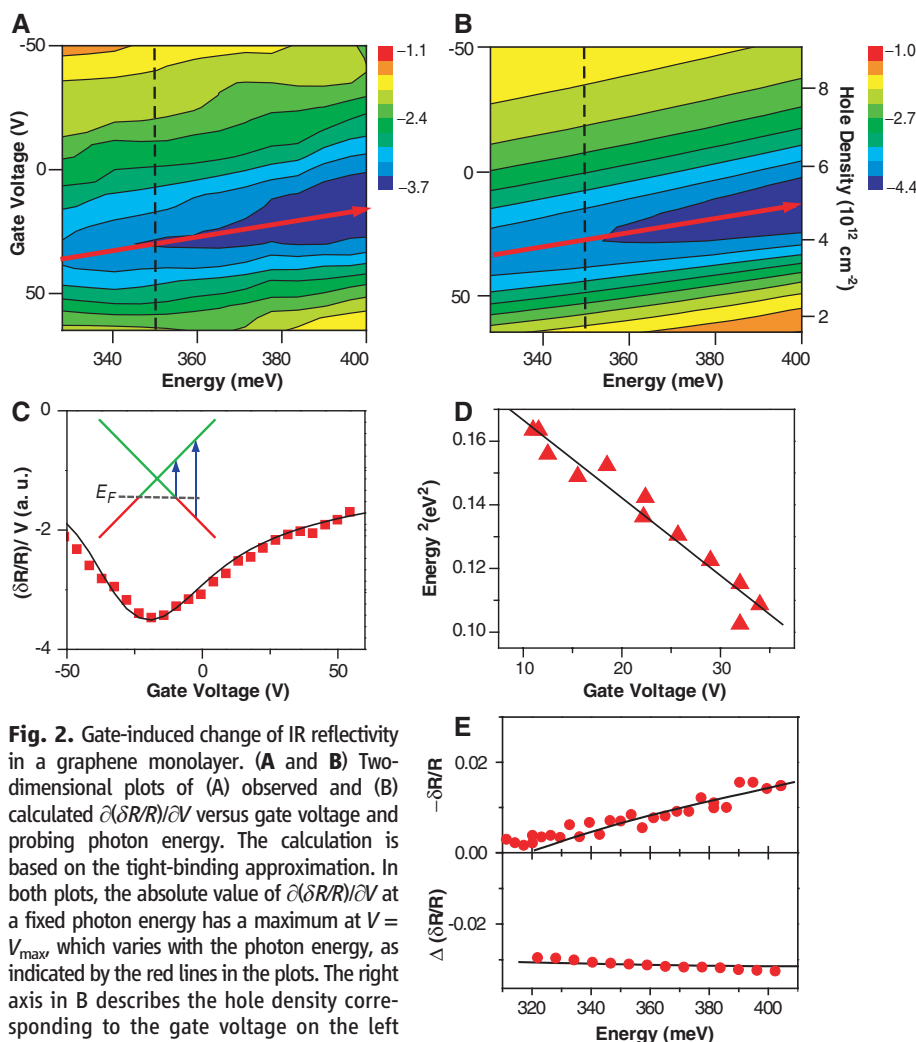


Fig. 2. Gate-induced change of IR reflectivity in a graphene monolayer. (A and B) Two-dimensional plots of (A) observed and (B) calculated $\partial(\delta R/R)/\partial V$ versus gate voltage and probing photon energy. The calculation is based on the tight-binding approximation. In both plots, the absolute value of $\partial(\delta R/R)/\partial V$ at a fixed photon energy has a maximum at $V = V_{\text{max}}$ which varies with the photon energy, as indicated by the red lines in the plots. The right axis in B describes the hole density corresponding to the gate voltage on the left axis. (C) A vertical line cut of the 2D plots at 350 meV, where the maximum modulation (in absolute value) is clearly observed. The inset illustrates interband transitions in graphene monolayers. E_F shifts upon gating, which affects the transitions. Gate-induced modification is strongest when the initial states for transitions are near the Fermi surface, i.e., $2|E_F| = \hbar\omega$. A small shift of E_F can block such transitions by changing the initial state from filled to empty, whereas transitions at significantly lower or higher energies are not affected. (D) The trace of maximum modulation plotted as squared photon energy versus gate voltage. Its slope yields directly the velocity dispersion of the Dirac band, $v_F = 8.1 \times 10^5$ m/s. (E) Experimental data (symbols) and model prediction (lines) of (upper panel) $-\delta R/R$ spectrum for an ungated graphene monolayer and (lower panel) the total gate-induced reflectivity spectrum change, $\Delta(\delta R/R)$, with gate voltage varied from -50 to 60 V. The magnitude of gate-induced reflectance change is larger than the initial monolayer reflectance.

voltage for the maximum signal decreases with the photon energy (red line in Fig. 2A).

The 2D spectra of graphene monolayers allow us to determine directly the electronic band dispersion. We consider the interband transitions illustrated in the inset of Fig. 2C. The applied gate voltage changes the charge-carrier density in graphene, $n = \alpha(V + V_0)$, and accordingly shifts E_F , where $E_F = \text{sgn}(n)\hbar v_F \sqrt{\pi|n|}$. Here, positive (negative) n means electron (hole) doping, v_F is the Fermi velocity, $\alpha \approx 7 \times 10^{10} \text{ cm}^{-2}\text{V}^{-1}$ (estimated from a simple capacitor model), and V_0 is the offset voltage caused by natural doping (which could vary from sample to sample) (1, 3). The shift in E_F affects the IR spectrum through the Drude response of the altered electron density and through the change of band filling (for example, a down shift of E_F eliminates transitions originating from initially occupied states right above the downshifted E_F).

The band-filling effect dominates at photon energy corresponding to transitions that originate from states near the Fermi surface, that is, $2|E_F| = \hbar\omega$. Thus, the trace for maximum $\partial(\delta R/R)/\partial V$ signal is defined by $\hbar\omega = 2\hbar v_F \sqrt{\alpha\pi|V + V_0|}$, and the slope of $(\hbar\omega)^2$ versus V yields directly the dispersion velocity of the Dirac band, $v_F = 0.8 \times 10^6$ m/s (Fig. 2D). Our value is comparable to that obtained by transport (1, 3) and by photoemission (23–25), and the small difference could be due to the uncertainty in our determination of gate-coupling efficiency.

To describe the gate-dependent spectra quantitatively, we use the tight-binding model (17, 18) to calculate the optical transitions and the frequency-dependent complex conductivity for different E_F . In this model, the Fermi velocity v_F is the only parameter needed to describe the band structure and optical transition matrix elements, and $V + V_0$ sets the Fermi energy level. We introduce an uncertainty ΔV_0 in V_0 to account for inhomogeneous doping of the sample. We can then calculate the spectrum of $\partial(\delta R/R)/\partial V$ for different V_0 using Eq. 1. The results with $v_F = 0.8 \times 10^6$ m/s, $V_0 = -70$ V, and $\Delta V_0 = \pm 16$ V are presented in Fig. 2B. They agree nicely with the experimental data in Fig. 2A (26).

The same model can be used to describe the ungated $-\delta R/R$ spectrum of the monolayer in Fig. 1A. The fitting is shown in the upper panel of Fig. 2E. We can compare it with the total gate-induced reflectivity change over the gate-voltage range of -50 to 60 V, $\Delta(\delta R/R) = (\delta R/R)|_{V_g=60\text{V}} - (\delta R/R)|_{V_g=-50\text{V}}$, displayed in the lower panel of Fig. 2E. The magnitude of $\Delta(\delta R/R)$ is obviously greater than reflection response, $-\delta R/R$, from the ungated monolayer. It follows from switch-off of IR transitions by electrical gating through a downshift of E_F .

The spectrum of gate-induced reflectance change, $\partial(\delta R/R)/\partial V$, for a graphene bilayer is shown in Fig. 3A. It exhibits features distinctly different from that of the monolayer (Fig. 2A). A clear peak exists in the modulation spectra,

which can be easily seen from a horizontal line cut in the 2D plot (symbols in Fig. 3C). Also, the signal at the peak has an opposite sign compared with that in the monolayer, indicating a fundamentally different mechanism.

Qualitatively, we can attribute this observation to the van Hove singularity associated with the optical transitions between parallel valence bands of a p-doped graphene bilayer, illustrated by the blue arrowed lines in the Fig. 3C inset. It leads to a peak in bilayer absorption at the band separation energy, and the peak becomes stronger with increasing hole concentration as E_F shifts down and more transitions become allowed. This situation is in contrast to the reduction of transition strength with down-shifting of the Fermi level in a graphene monolayer, which gives an opposite sign to $\partial(\delta R/R)/\partial V$. Transitions between other bands (black arrowed lines in the illustration in Fig. 3C) are also affected by gating, and a small band gap is expected to appear because of asymmetry of the gating effect on the upper and the lower layers of the bilayer

(21, 27). However, there is no strong van Hove singularity involved, and therefore these transitions contribute only to an overall slowly varying background.

To be more quantitative, we model the bilayer using the tight-binding approximation, following (19), to calculate the complex conductivity. We use the same set of parameter values as in the monolayer case but include the interlayer hopping rate γ_1 as an additional parameter to take into account the interlayer coupling. The best fit of the spectral variation with gate voltage from our calculation is shown in Fig. 3B; a horizontal line cut of the 2D plot is given in Fig. 3C to compare with the experimental data. The fit yields $\gamma_1 = 350$ meV and $V_0 = -50$ V from natural doping, assuming that all the dopants appear at the upper surface of the bilayer.

Comparisons between theory and experiment in Fig. 3, A and B, show that the main experimental features are reproduced by the model. However, significant deviations exist, such as the slight difference in peak energies and in

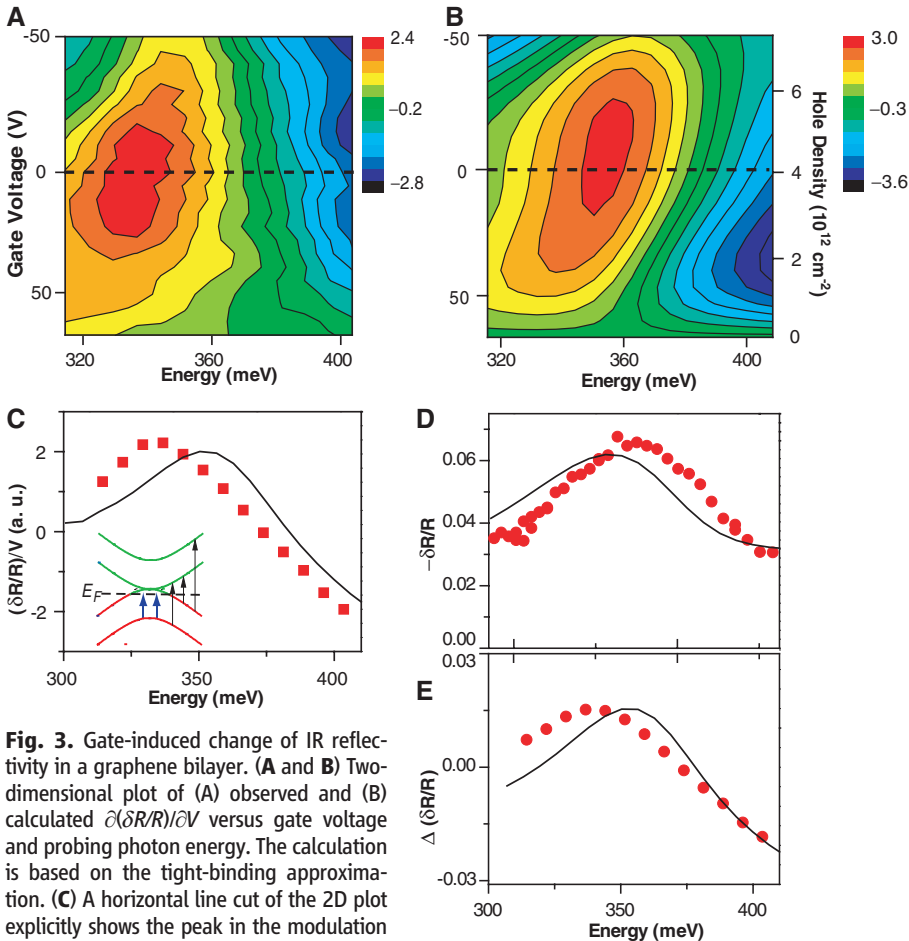


Fig. 3. Gate-induced change of IR reflectivity in a graphene bilayer. (A and B) Two-dimensional plot of (A) observed and (B) calculated $\partial(\delta R/R)/\partial V$ versus gate voltage and probing photon energy. The calculation is based on the tight-binding approximation. (C) A horizontal line cut of the 2D plot explicitly shows the peak in the modulation spectra. Symbols are experimental data, and the line is from the model prediction. The inset illustrates the interband transitions in bilayers. Transitions between the parallel valence bands of the hole-doped bilayer, denoted by the red arrowed lines, give rise to a van Hove singularity and the observed spectral peak. Other interband transitions (black arrowed lines) contribute to a relatively flat response over the spectral range. (D and E) Experimental data (symbols) and model prediction (lines) of (D) $-\delta R/R$ spectrum for an ungated graphene bilayer and (E) the total gate-induced reflectivity spectrum change, $\Delta(\delta R/R)$, with gate voltage varied from -50 to 60 V. The gate-induced change of reflectance is of the same order of magnitude as the initial graphene reflectance.

gate dependences at spectral range from 370 to 400 meV. Also, our observed peak energy, ~ 350 meV, is close to, but smaller than, the energy separation of the parallel bands of 400 meV determined by photoemission measurements (21, 23). These discrepancies could arise from strong many-body effects in the bilayer excited state. For instance, excitonic effects can modify the optical spectrum appreciably, whereas photoemission probes quasiparticle transitions in the absence of excitons. Such excitonic behavior in a graphene bilayer could be quite unusual, considering the existence of parallel bands and the associated van Hove singularity.

Next, we compare the ungated $-\delta R/R$ spectrum in a graphene bilayer (Fig. 3D) and the spectrum of the total gate-induced change, $\Delta(\delta R/R) = (\delta R/R)|_{V_g=60V} - (\delta R/R)|_{V_g=-50V}$ (Fig. 3E). Again, $\Delta(\delta R/R)$ is comparable in magnitude to $\delta R/R$.

Our study reveals rich IR optical behaviors in graphene monolayers and bilayers. The observed interband transitions are quite strong: Although only one or two atoms thick, the graphene monolayer and bilayer can absorb, respectively, more than 2% and 6% (peak value) of normally incident IR radiation. In comparison, a 10-nm-thick GaAs layer absorbs about 1% of the light near the band gap. Using multiply stacked graphene sheets or optical multipasses or waveguiding, the IR response of graphene can be considerable: for example, IR light propagating along a 100- μm -long waveguide on undoped graphene would be completely absorbed. With the tunability provided by electrical gating and charge injection, one might envision novel graphene-based optoelectronics devices such as tunable IR detectors, modulators, and emitters.

References and Notes

1. K. S. Novoselov *et al.*, *Nature* **438**, 197 (2005).
2. K. S. Novoselov *et al.*, *Nat. Phys.* **2**, 177 (2006).
3. Y. B. Zhang, Y. W. Tan, H. L. Stormer, P. Kim, *Nature* **438**, 201 (2005).
4. M. I. Katsnelson, K. S. Novoselov, A. K. Geim, *Nat. Phys.* **2**, 620 (2006).
5. F. Miao *et al.*, *Science* **317**, 1530 (2007).
6. A. C. Ferrari *et al.*, *Phys. Rev. Lett.* **97**, 187401 (2006).
7. J. Yan, Y. B. Zhang, P. Kim, A. Pinczuk, *Phys. Rev. Lett.* **98**, 166802 (2007).
8. Z. Jiang *et al.*, *Phys. Rev. Lett.* **98**, 197403 (2007).
9. C. Casiraghi *et al.*, *Nano Lett.* **7**, 2711 (2007).
10. S. M. Bachilo *et al.*, *Science* **298**, 2361 (2002).
11. F. Wang, G. Dukovic, L. E. Brus, T. F. Heinz, *Science* **308**, 838 (2005).
12. K. S. Novoselov *et al.*, *Science* **306**, 666 (2004).
13. B. Huard *et al.*, *Phys. Rev. Lett.* **98**, 236803 (2007).
14. J. R. Williams, L. DiCarlo, C. M. Marcus, *Science* **317**, 638 (2007).
15. Tunable IR radiation was generated by an optical parametric amplifier pumped by a femtosecond Ti:sapphire amplifier system. The IR pulses were attenuated to ~ 1 nJ and spectrally narrowed through a monochromator to ~ 10 cm^{-1} before they were focused onto the graphene samples. The back-reflected light was collected and detected by a mercury cadmium telluride detector. The samples had a typical lateral dimension around 20 μm . The microscope we used had a 36 \times reflective objective that confined the infrared beam to a diameter < 10 μm on the sample.
16. See supporting material on Science Online.

17. V. P. Gusynin, S. G. Sharapov, J. P. Carbotte, *Phys. Rev. Lett.* **96**, 256802 (2006).
18. L. Falkovsky, A. Varlamov, <http://arxiv.org/abs/cond-mat/0606800> (2006).
19. E. V. Castro *et al.*, <http://arxiv.org/abs/cond-mat/0611342> (2006).
20. D. S. L. Abergel, V. I. Fal'ko, <http://arxiv.org/abs/cond-mat/0610673> (2007).
21. T. Ohta, A. Bostwick, T. Seyller, K. Horn, E. Rotenberg, *Science* **313**, 951 (2006).
22. A small band gap can open in a doped graphene bilayer (20). At our doping level, the bandgap is relatively small and will not affect the qualitative behaviors. In the tight binding calculation described in the text, this gap-opening effect is included in a self-consistent way following (16).
23. S. Y. Zhou *et al.*, *Nat. Mater.* **6**, 770 (2007).
24. A. Bostwick, T. Ohta, T. Seyller, K. Horn, E. Rotenberg, *Nat. Phys.* **3**, 36 (2007).
25. S. Y. Zhou *et al.*, *Nat. Phys.* **2**, 595 (2006).
26. The electron density of the Si back gate will also be modulated by electrical gating. It will also contribute to the IR reflectivity change and is described by Drude free-carrier response. However, its contribution is more than an order of magnitude smaller than that of graphene and remains a constant at different dc gate voltages.
27. E. McCann, <http://arxiv.org/abs/cond-mat/0608221> (2006).
28. We thank S. Louie and Y. Li for helpful discussions. This work was supported by the Office of Basic

Energy Sciences, U.S. Department of Energy, under contract DE-AC03-76SF0098. F.W. and Y.Z. acknowledge the support from the Miller Institute for Miller research fellowships, and C.T. acknowledges support from a NSF grant through Water CAMPWS CTS-0120978.

Supporting Online Material

www.sciencemag.org/cgi/content/full/1152793/DC1
SOM Text

8 November 2007; accepted 3 March 2008
Published online 13 March 2008;
10.1126/science.1152793
Include this information when citing this paper.

Current-Controlled Magnetic Domain-Wall Nanowire Shift Register

Masamitsu Hayashi, Luc Thomas, Rai Moriya, Charles Rettner, Stuart S. P. Parkin*

The controlled motion of a series of domain walls along magnetic nanowires using spin-polarized current pulses is the essential ingredient of the proposed magnetic racetrack memory, a new class of potential non-volatile storage-class memories. Using permalloy nanowires, we achieved the successive creation, motion, and detection of domain walls by using sequences of properly timed, nanosecond-long, spin-polarized current pulses. The cycle time for the writing and shifting of the domain walls was a few tens of nanoseconds. Our results illustrate the basic concept of a magnetic shift register that relies on the phenomenon of spin-momentum transfer to move series of closely spaced domain walls.

More than three decades ago, the concept of storing information in movable domain walls (DWs) was introduced, and the following years saw intense interest in “magnetic bubble memories” (1). The magnetic bubbles were often arranged in the form of shift registers and manipulated with fixed and alternating magnetic fields (2). However, this required on-chip field generators at the same size scale as the individual magnetic bits, adding considerable complexity and cost to the device and making scaling to smaller dimensions very difficult (3). These obstacles can be overcome by taking advantage of the interaction of spin-polarized current with magnetization in the DWs, which results in a spin-transfer torque on the DW, causing it to move (4–9). This effect has been observed in a number of magnetic materials (10–13), but predominantly in permalloy ($\text{Ni}_{81}\text{Fe}_{19}$) nanowires (14–17). The use of spin-momentum transfer considerably simplifies the memory device because the current is passed directly across the DW without the need for any additional field generators.

In a permalloy nanowire in which the magnetization lies along the nanowire, adjacent DWs alternate between head-to-head (HH) and tail-to-

tail (TT) configurations (Fig. 1, B and C). Under the application of a uniform magnetic field, these DWs will move in opposite directions, leading to their potential annihilation. In contrast, spin-polarized current can, in principle, move a series of neighboring DWs in the same direction. Moreover, spin-momentum transfer becomes more efficient the smaller the size of the magnetic element is (18). We describe here the basic working principle of a current-controlled magnetic DW shift register, the fundamental building block of magnetic racetrack memory (19).

In a scanning electron microscopy (SEM) image of a typical permalloy nanowire (Fig. 1A), three pulse generators (PG-1, PG-2, and PG-3) are connected to electrical contact lines A and B, spaced 6 μm apart (20) (SOM text A). The resistance of the nanowire was measured to determine whether a DW was present in the region between line A and B (section A-B). The nanowire resistance also provides information about the structure of the DW (21); that is, whether it is a transverse or a vortex DW (22). In these DWs, the magnetization largely lies in the plane of the nanowire. In the transverse case the magnetization rotates about an axis perpendicular to the length of the nanowire, whereas in the vortex case, the magnetization rotates about a tiny core in which a small net moment points into or out of the plane of the nanowire (Fig. 2 D).

A voltage pulse from one of the pulse generators (PG-1 or PG-2) was used to inject a

current into line A as well as into the nanowire. The current that passes through line A generates a highly localized magnetic field that, when sufficiently large and when the magnetization of the nanowire is properly aligned, creates a DW in section A-B. The current that flows into the nanowire drives the DW along the nanowire between A and B in a direction determined by the current flow direction. The nanowire was first magnetized along the $-(+)$ X direction with an external magnetic field $H = -(+)$ 300 Oe, which was then set as close as possible to zero ($|H| < \sim 0.3$ Oe, unless otherwise noted). A HH (or TT) DW was subsequently created in section A-B when a negative voltage pulse was injected from PG-2 (PG-1). Throughout this study, the amplitude of the voltage pulse from PG-1 and PG-2 was fixed at -3.2 V.

Previous experiments showed that the DW created in section A-B moves along the nanowire and exits from line B only when the pulse length exceeds a threshold value τ_p . This pulse length is determined by the DW velocity, which depended on the current density flowing along the nanowire, and H (17). Only vortex and not transverse DWs could be moved with current under the experimental conditions used (8, 16, 17). For example, the probability of finding a vortex wall in section A-B is plotted as a function of the pulse length (Fig. 1, B and C) for TT and HH walls, respectively, for a current density of $\sim -2.0 \times 10^8$ A/cm². For both walls, $\tau_p \sim 35$ ns.

When the injection pulse length is shorter than τ_p , we hypothesized that the DW would move along the nanowire a distance in proportion to the pulse length. This was verified by using an ejection voltage pulse to determine the time needed to move the DW either backward to A or forward to B as a function of the injection pulse length. The ejection pulse was applied from PG-3 to line B with an amplitude of $\sim \pm 1.6$ V, which corresponds to a current of $\sim \mp 2 \times 10^8$ A/cm² in the nanowire; that is, nearly equal to that of the injection pulse current density (fig. S1). Positive voltage applied to line B provides spin-transfer torque, which pushes the DW along the $+X$ direction, whereas negative voltage pushes it in the $-X$ direction.

The pulse length required to eject the DW from the nanowire is plotted as a function of the

IBM Research Division, Almaden Research Center, San Jose, CA 95120, USA.

*To whom correspondence should be addressed. E-mail: parkin@almaden.ibm.com